

# The Microwave Background Bispectrum

## Paper I: Basic Formalism

David N. Spergel and David M. Goldberg  
Princeton University Observatory, Princeton, NJ 08544

May 27, 2022

### Abstract

In this paper, we discuss the potential importance of measuring the CMB anisotropy bispectrum. We develop a formalism for computing the bispectrum and for measuring it from microwave background maps. As an example, we compute the bispectrum resulting from the 2nd order Rees-Sciama effect, and find that is undetectable with current and upcoming missions.

## 1 Introduction

Observations of microwave background fluctuations are a powerful probe of the physical conditions in the early universe. Most analyses of the microwave background focus on measuring and interpreting the two-point function. If the microwave background fluctuations were a purely Gaussian random field, then the two-point function would completely characterize the microwave background. The non-linear growth of structure produces non-Gaussian fluctuations. If detectable, these non-Gaussian fluctuations are a new window into the evolution and growth of structure.

The three-point function and its analog, the bispectrum, are potential tools for detecting these non-linear effects. At present, there is no clear signature of such modes. There was no detection of three point correlations in the COBE data, nor any topological signatures of non-Gaussianity[1]. While

there is a reported detection of non-Gaussianity in the COBE bispectrum[2, 3]. Our ability to detect these effects will soon improve by many orders of magnitude with the launch of the MAP satellite[4] and the PLANCK[5] satellite. These upcoming launches motivate our detailed study of the bispectrum and the three-point function.

In this article, we first discuss why the bispectrum is interesting (§ 2), develop a general form for calculating the bispectrum (§ 3) and then discuss the particular case of those perturbations resulting from the Rees-Sciama effect (§ 4). While the Rees-Sciama bispectrum is not detectable, we show in a companion paper that the non-Gaussian effects produced at low redshift through a coupling of gravitational lensing and either the Sunyaev-Zel'dovich effect or the late time ISW effect produces a detectable signal.

## 2 Why is the Bispectrum Interesting?

The three-point function and its transform, the bispectrum, are potential tools for detecting non-Gaussianity in the microwave sky. Just as the multipole spectrum is a useful statistic for studying the two-point correlation, the bispectrum is useful in studying the three-point function. To put this in context, we define the  $a_{lm}$  as the expansion of the temperature anisotropies into spherical harmonics:

$$a_{lm} \equiv \int d\hat{\mathbf{n}} T(\hat{\mathbf{n}}) Y_{lm}^*(\hat{\mathbf{n}}) \quad (1)$$

Thus, since the three point function is defined as  $B(\hat{\mathbf{l}}, \hat{\mathbf{m}}, \hat{\mathbf{n}}) \equiv T(\hat{\mathbf{l}})T(\hat{\mathbf{m}})T(\hat{\mathbf{n}})$ , we define the bispectrum as:

$$B_{l_1 l_2 l_3}^{m_1 m_2 m_3} = a_{l_1 m_1} a_{l_2 m_2} a_{l_3 m_3} \quad (2)$$

The universe is thought to be rotationally invariant, and hence, a more useful quantity is the angle-averaged bispectrum:

$$B_{l_1 l_2 l_3} = \sum_{m_1, m_2, m_3} \begin{pmatrix} l_1 & l_2 & l_3 \\ m_1 & m_2 & m_3 \end{pmatrix} B_{l_1 l_2 l_3}^{m_1 m_2 m_3} \quad (3)$$

Even if there was no non-Gaussianity in the initial potential fluctuations, non-linear physics will produce mode-mode couplings. We argue here that the bispectrum is a particularly powerful tool for detecting these couplings.

In inflation, quantum fluctuations produce Gaussian random phase variations in the gravitational potential:

$$\Phi(\mathbf{x}) = \int \frac{d^3\mathbf{k}}{(2\pi)^3} \Phi_0(\mathbf{k}) \exp(i\mathbf{k} \cdot \mathbf{x}) \quad (4)$$

with  $\langle \Phi_0(\mathbf{k}) \Phi_0^*(\mathbf{k}') \rangle = P(k) \delta^{(3)}(\mathbf{k} - \mathbf{k}')$ , the power spectrum of potential fluctuations at the current epoch. While processes during inflation may produce some non-Gaussianity, this is small in most inflationary models [6]. On the other hand, when the fluctuations reenter the horizon, there are many non-linear effects that alter these initial conditions. Near decoupling, non-linear hydrodynamical effects couple modes [7]. After decoupling, non-linear general relativistic corrections also alter the microwave background spectrum [8, 9] as do non-linear coupling between density fluctuations [10, 11]. However, since potential fluctuations in the early universe are small,  $\langle \Phi^2 \rangle \sim 10^{-9}$ , these non-linear effects are usually viewed as undetectable. For example, Mollerach et al. [10] and Munshi et al. [11] estimated the reduced bispectrum generated by non-linear evolution of long wavelength modes and showed that they are undetectable in the COBE maps. In a spatially flat universe, the microwave background temperature at the surface of last scatter can be linearly related to the potential fluctuations at that epoch, giving us what we shall henceforth call the linear temperature approximation:

$$T^L(\hat{\mathbf{n}}) = \phi(\tau_r) \int \frac{d^3\mathbf{k}}{(2\pi)^3} e^{i\mathbf{k} \cdot \hat{\mathbf{n}} \tau_r} \Phi_0(\mathbf{k}) g(k), \quad (5)$$

where  $\tau$  is the comoving (conformal) lookback time,  $\phi(\tau)$  is a normalization constant for potential perturbations which is equal to unity today, and  $g(k)$  is the linear radiation transfer function and describes the relationship between potential fluctuations and temperature fluctuations at recombination. For small  $k$ ,  $g(k) = 1/3$ . For larger  $k$ , we need to evolve the coupled matter-radiation fluid. Codes like CMBFAST compute  $g(k)$  for different cosmological models.

Expanding the linear part of the temperature perturbation into spherical harmonics:

$$a_{lm}^L = \phi(\tau_r) \int \frac{d^3\mathbf{k}}{(2\pi)^3} d\hat{\mathbf{n}} e^{i\mathbf{k} \cdot \hat{\mathbf{n}} \tau_r} \Phi_0(\mathbf{k}) g(k) Y_{lm}^*(\hat{\mathbf{n}}). \quad (6)$$

Since we will later wish to integrate over the sky, it will be useful to expand out the exponential into spherical harmonics as well using the Rayleigh expansion:

$$e^{i\mathbf{k}\cdot\mathbf{r}} = 4\pi \sum_{lm} i^l j_l(kr) Y_{lm}^*(\hat{\mathbf{r}}) Y_{lm}(\hat{\mathbf{k}}) . \quad (7)$$

Thus, the linear approximation of the CMB fluctuations are given by:

$$a_{lm}^L = 4\pi\phi(\tau_r)(-i)^l \int \frac{d^3\mathbf{k}}{(2\pi)^3} \Phi_0(\vec{k}) Y_{l,-m}(\hat{\mathbf{k}}) j_l(k\tau_r) g(k) \quad (8)$$

In addition to the terms proportional to  $\Phi_0(\mathbf{k})$  (linear), there are a number of terms in the temperature fluctuations which are proportional to  $\Phi_0(\mathbf{k})^2$  (nonlinear). These corrections arise from gravitational couplings, gravitational lensing, and radiation effects. These terms generically add a correction to the microwave background:

$$\begin{aligned} T^{NL}(\hat{\mathbf{n}}) &= \int_{\tau_r}^0 d\tau \Phi^2(\hat{\mathbf{n}}) f(\hat{\mathbf{n}}\tau, \tau) \\ &= \int d\tau \phi^2(\tau) \int \frac{d^3\mathbf{k}_1}{(2\pi)^3} \frac{d^3\mathbf{k}_2}{(2\pi)^3} \Phi_0(\mathbf{k}_1) \Phi_0(\mathbf{k}_2) e^{i(\mathbf{k}_1+\mathbf{k}_2)\cdot\hat{\mathbf{n}}\tau} f(\mathbf{k}_1, \mathbf{k}_2, \tau) \end{aligned} \quad (9)$$

We may again take the spherical harmonic transform of the non-linear temperature perturbation to calculate the coefficient,  $a_{lm}^{NL}$ . We will find it convenient to expand the coupling term,  $f(\mathbf{k}_1, \mathbf{k}_2, \tau)$  into Legendre polynomials:

$$f(\mathbf{k}_1, \mathbf{k}_2, \tau) \equiv \sum_l f_l(k_1, k_2, \tau) P_l(\hat{\mathbf{k}}_1 \cdot \hat{\mathbf{k}}_2) = \sum_{lm} \frac{4\pi}{2l+1} f_l(k_1, k_2, \tau) Y_{lm}(\hat{\mathbf{k}}_1) Y_{lm}^*(\hat{\mathbf{k}}_2) \quad (10)$$

Since the non-linear term will only couple to itself if  $\mathbf{k}_1 = \mathbf{k}_2$ , we can safely ignore this effect, and instead concentrate on the case in which a bispectrum is produced by:

$$B_{m_1 m_2 m_3}^{l_1 l_2 l_3} = a_{l_1 m_1}^L a_{l_2 m_2}^L a_{l_3 m_3}^{NL*} + a_{l_2 m_2}^L a_{l_3 m_3}^L a_{l_1 m_1}^{NL*} + a_{l_3 m_3}^L a_{l_1 m_1}^L a_{l_2 m_2}^{NL*} \quad (11)$$

We will only examine the first term in this derivation, and add in the other two permutation in the end.

Looking at  $a_{l_3 m_3}^{NL*}$ , we find:

$$\begin{aligned}
a_{l_3 m_3}^{NL*} &= \frac{(4\pi)^3}{(2\pi)^6} \int d\tau \phi^2(\tau) \int k_1^2 dk_1 k_2^2 dk_2 \Phi_0^*(\mathbf{k}_1) \Phi_0^*(\mathbf{k}_2) \\
&\times \sum_{l'l''mm'm''} (-i)^{l'+l''} \frac{1}{2l+1} f_l(k_1, k_2, \tau) j_{l'}(k_1\tau) j_{l''}(k_2\tau) \\
&\times \int d\hat{\mathbf{n}} d\hat{\mathbf{k}}_1 d\hat{\mathbf{k}}_2 Y_{l_3 m_3}(\hat{\mathbf{n}}) Y_{l'm'}(\hat{\mathbf{n}}) Y_{l''m''}(\hat{\mathbf{n}}) Y_{l'm'}^*(\hat{\mathbf{k}}_1) Y_{lm}^*(\hat{\mathbf{k}}_1) Y_{lm}(\hat{\mathbf{k}}_2) Y_{l''m''}^*(\hat{\mathbf{k}}_2)
\end{aligned} \tag{12}$$

Substituting this expression and equation (8) into equation (11), we get:

$$\begin{aligned}
a_{l_1 m_1}^L a_{l_2 m_2}^L a_{l_3 m_3}^{NL*} &= \frac{(4\pi)^5}{(2\pi)^6} \phi^2(\tau_r) \int d\tau \phi^2(\tau) \int \frac{d^3\mathbf{k}}{(2\pi)^3} \frac{d^3\mathbf{k}'}{(2\pi)^3} \int k_1^2 dk_1 k_2^2 dk_2 \\
&\times \Phi_0(\mathbf{k}) \Phi_0(\mathbf{k}') \Phi_0^*(\mathbf{k}_1) \Phi_0^*(\mathbf{k}_2) g(k) g(k') \\
&\times \sum_{l'l''mm'm''} \frac{1}{2l+1} f_l(k_1, k_2, \tau) j_{l'}(k_1\tau) j_{l''}(k_2\tau) j_{l_1}(k\tau_r) j_{l_2}(k'\tau_r) \\
&\times \int d\hat{\mathbf{n}} d\hat{\mathbf{k}}_1 d\hat{\mathbf{k}}_2 Y_{l_3 m_3}(\hat{\mathbf{n}}) Y_{l'm'}(\hat{\mathbf{n}}) Y_{l''m''}(\hat{\mathbf{n}}) Y_{l'm'}^*(\hat{\mathbf{k}}_1) Y_{lm}^*(\hat{\mathbf{k}}_1) Y_{l_1 m_1}^*(\hat{\mathbf{k}}) \\
&\times \int d\hat{\mathbf{k}}_2 Y_{lm}(\hat{\mathbf{k}}_2) Y_{l''m''}^*(\hat{\mathbf{k}}_2) Y_{l_2 m_2}^*(\hat{\mathbf{k}}')
\end{aligned} \tag{13}$$

The integrals over  $\mathbf{k}$  and  $\mathbf{k}'$  give two possible permutations,  $\delta(\mathbf{k} - \mathbf{k}_1)$  and  $\delta(\mathbf{k} - \mathbf{k}_2)$ . This is patently symmetric, and thus, we will chose the former and multiply the integral by 2. After integrating over  $\mathbf{k}$  and  $\mathbf{k}'$ , we find that we have 3 sets of 3 spherical harmonics. This is precisely the form of the  $Q$  coefficients discussed in the appendix. Thus, integrating over  $\hat{\mathbf{n}}$ ,  $\hat{\mathbf{k}}_1$ , and  $\hat{\mathbf{k}}_2$ , summing over  $m, m', m''$ , and convolving with the Wigner 3-j symbol over  $m_1, m_2, m_3$  as in equation (3), we find that the first of three terms in the angle averaged bispectrum is:

$$\begin{aligned}
B_{l_1 l_2 l_3}^{(1)} &= \frac{1}{2\pi^4} \phi^2(\tau_r) \int d\tau \phi^2(\tau) \int dk_1 dk_2 k_1^2 k_2^2 P(k_1) P(k_2) g(k_1) g(k_2) \\
&\times \sum_{l'l''} (2l'+1)(2l''+1) Q_{l'l''}^{l_1 l_2 l_3} f_l(k_1, k_2, \tau) j_{l'}(k_1\tau) j_{l''}(k_2\tau) j_{l_1}(k_1\tau_r) j_{l_2}(k_2\tau_r)
\end{aligned} \tag{14}$$

### 3 Measuring the Bispectrum

Measuring this effect from observations is quite straightforward. If there is complete sky coverage and no sky cuts, the the angle averaged bispectrum

can be computed by rewriting the Wigner 3-j symbols as integrals over the sky,

$$\begin{aligned}
\begin{pmatrix} l_1 & l_2 & l_3 \\ 0 & 0 & 0 \end{pmatrix} B_{l_1 l_2 l_3} &= \sum_{m_1, m_2, m_3} \begin{pmatrix} l_1 & l_2 & l_3 \\ 0 & 0 & 0 \end{pmatrix} \begin{pmatrix} l_1 & l_2 & l_3 \\ m_1 & m_2 & m_3 \end{pmatrix} a_{l_1 m_1} a_{l_2 m_2} a_{l_3 m_3} \\
&= \sqrt{\frac{(4\pi)^3}{(2l_1 + 1)(2l_2 + 1)(2l_3 + 1)}} \\
&\quad \times \sum_{m_1, m_2, m_3} \int d\hat{\mathbf{q}} Y_{l_1 m_1}(\hat{\mathbf{q}}) Y_{l_2 m_2}(\hat{\mathbf{q}}) Y_{l_3 m_3}(\hat{\mathbf{q}}) \\
&\quad \times \int d\hat{\mathbf{l}} d\hat{\mathbf{m}} d\hat{\mathbf{n}} Y_{l_1 m_1}^*(\hat{\mathbf{l}}) Y_{l_2 m_2}^*(\hat{\mathbf{m}}) Y_{l_3 m_3}^*(\hat{\mathbf{n}}) T(\hat{\mathbf{l}}) T(\hat{\mathbf{m}}) T(\hat{\mathbf{n}}) \\
&= \int d\hat{\mathbf{q}} e_{l_1}(\hat{\mathbf{q}}) e_{l_2}(\hat{\mathbf{q}}) e_{l_3}(\hat{\mathbf{q}}) \tag{15}
\end{aligned}$$

where the sky map is averaged over rings centered around point  $\hat{\mathbf{q}}$ :

$$e_l(\hat{\mathbf{q}}) = \sqrt{\frac{2l+1}{4\pi}} \int d\hat{\mathbf{l}} T(\hat{\mathbf{l}}) P_l(\hat{\mathbf{q}} \cdot \hat{\mathbf{l}}) \tag{16}$$

Since the bispectrum signal is rather weak, the dominant source of noise is the cosmic variance of the dominant Gaussian signal. For a Gaussian random field,  $\langle a_{l_1 m_1} a_{l_2 m_2} a_{l_3 m_3} \rangle = 0$ . However, its variance,  $\langle (a_{l_1 m_1} a_{l_2 m_2} a_{l_3 m_3})^2 \rangle = c_{l_1} c_{l_2} c_{l_3}$  for  $l_1 \neq l_2$ ,  $l_2 \neq l_3$ ,  $l_1 \neq l_3$  [12]. When we include detector noise, then

$$\langle (a_{l_1 m_1} a_{l_2 m_2} a_{l_3 m_3})^2 \rangle = (c_{l_1} + \sigma_0^2 w_{l_1}^{-2}) (c_{l_2} + \sigma_0^2 w_{l_2}^{-2}) (c_{l_3} + \sigma_0^2 w_{l_3}^{-2}) \tag{17}$$

where  $\sigma_0$  is the detector noise and  $w_l$  is the experimental window function. Similarly, for a Gaussian field,

$$\begin{aligned}
\langle B_{l_1 l_2 l_3} \rangle &= 0 \\
\langle B_{l_1 l_2 l_3} B_{l'_1 l'_2 l'_3} \rangle &= (c_{l_1} + \sigma_0^2 w_{l_1}^{-2}) (c_{l_2} + \sigma_0^2 w_{l_2}^{-2}) (c_{l_3} + \sigma_0^2 w_{l_3}^{-2}) \\
&\quad \times (\delta_{l_1 l'_1} \delta_{l_2 l'_2} \delta_{l_3 l'_3} + \delta_{l_1 l'_2} \delta_{l_2 l'_1} \delta_{l_3 l'_3} + \delta_{l_1 l'_3} \delta_{l_2 l'_2} \delta_{l_3 l'_1} + \delta_{l_1 l'_1} \delta_{l_2 l'_3} \delta_{l_3 l'_2} + \delta_{l_1 l'_2} \delta_{l_2 l'_3} \delta_{l_3 l'_1} + \delta_{l_1 l'_3} \delta_{l_2 l'_1} \delta_{l_3 l'_2})
\end{aligned} \tag{18}$$

for  $l_1 \neq l_2$ ,  $l_2 \neq l_3$ ,  $l_1 \neq l_3$ . Because of this symmetry, we restrict ourselves to bispectrum terms where  $l_1 < l_2 < l_3$ .

## 4 The Bispectrum from the Rees-Sciama Effect

Several groups[10, 11] have discussed the possibility of detecting the non-linear signature of the Rees-Sciama effect in the COBE data. They concluded that the signal was undetectable on COBE scales. In their analysis, they focus only on the diagonal terms in the bispectrum. Here, we compute the predicted signal on smaller angular scales and compute all of the bispectrum terms.

The second order Rees-Sciama effect arises from the non-linear growth of density fluctuations[10]:

$$\begin{aligned} T^{NL}(\hat{\mathbf{n}}) &= 2 \int d\tau \frac{\partial}{\partial \tau} \Phi^{NL}(\hat{\mathbf{n}}\tau, \tau) \\ &= 2 \int d\tau \frac{\partial}{\partial \tau} \int \frac{d^3 \mathbf{k}}{(2\pi)^3} \Phi^{NL}(\hat{\mathbf{k}}, \tau) e^{i\mathbf{k} \cdot \hat{\mathbf{n}}\tau} \end{aligned} \quad (19)$$

and give the second-order potential perturbation as:

$$\Phi^{NL}(\mathbf{k}, \tau) = -\frac{(\tau_0 - \tau)^2}{84k^2} \phi^2(\tau) \int \frac{d^3 \mathbf{k}'}{(2\pi)^3} \Phi_0(\mathbf{k} - \mathbf{k}') \Phi_0(\mathbf{k}') [3k^2 k'^2 + 7k^2 \mathbf{k} \cdot \mathbf{k}' - 10(\mathbf{k} \cdot \mathbf{k}')^2] \quad (20)$$

This second-order approximation is valid for  $k < 1h \text{ Mpc}^{-1}$ . [13].

Since we expect much of the signal to come from high redshift contributions, and since in a flat,  $\Omega_m = 1$  universe,  $\dot{\phi}(\tau) = 0$ , we will take  $\phi(\tau)$  is constant for the remainder of this derivation. Additionally, we will redefine our variables of integration:  $\mathbf{k}_1 \equiv \mathbf{k} - \mathbf{k}'$  and  $\mathbf{k}_2 = \mathbf{k}'$ . This yields:

$$\begin{aligned} T^{NL}(\hat{\mathbf{n}}) &= \int d\tau \phi^2(\tau) \int \frac{d^3 \mathbf{k}_1}{(2\pi)^3} \frac{d^3 \mathbf{k}_2}{(2\pi)^3} \Phi_0(\mathbf{k}_1) \Phi_0(\mathbf{k}_2) e^{i(\mathbf{k}_1 + \mathbf{k}_2) \cdot \hat{\mathbf{n}}\tau} \\ &\times \frac{(\tau_0 - \tau)}{21(\mathbf{k}_1 + \mathbf{k}_2)^2} [10k_1^2 k_2^2 + 7(k_1^2 + k_2^2)k_1 k_2 \mu + 4k_1^2 k_2^2 \mu^2] \end{aligned} \quad (21)$$

where  $\mu \equiv \hat{\mathbf{k}}_1 \cdot \hat{\mathbf{k}}_2$ .

The second part of the equation is the coupling function,  $f(\hat{\mathbf{k}}_1, \hat{\mathbf{k}}_2, \tau)$ . The vectors in the denominator make it difficult to decompose it into Legendre polynomials, however, this may be simplified by noting that:

$$a_{lm}^{NL} \propto \int d\hat{\mathbf{n}} e^{i(\mathbf{k}_1 + \mathbf{k}_2) \cdot \hat{\mathbf{n}}\tau} Y_{lm}^*(\hat{\mathbf{n}}) \quad (22)$$

Thus, taking the Laplacian of  $a_{lm}^{NL}$ , we find:

$$l(l+1)a_{lm}^{NL*} = \int d\hat{\mathbf{n}} \int d\tau \phi^2(\tau) \int \frac{d^3\mathbf{k}_1}{(2\pi)^3} \frac{d^3\mathbf{k}_2}{(2\pi)^3} \Phi_0(\mathbf{k}_1) \Phi_0(\mathbf{k}_2) e^{i(\mathbf{k}_1+\mathbf{k}_2)\cdot\hat{\mathbf{n}}\tau} Y_{lm}^{NL}(\hat{\mathbf{n}}) \\ \times f(\mathbf{k}_1, \mathbf{k}_2, \tau) (\mathbf{k}_1 + \mathbf{k}_2)^2 \tau^2 \quad (23)$$

We now define a new coupling function:

$$\tilde{f}(\mathbf{k}_1, \mathbf{k}_2, \tau) \equiv f(\mathbf{k}_1, \mathbf{k}_2, \tau) (\mathbf{k}_1 + \mathbf{k}_2)^2 \tau^2, \quad (24)$$

which can be easily substituted into the definition of the bispectrum, with  $B_{l_1 l_2 l_3} \Rightarrow l_3(l_3+1)B_{l_1 l_2 l_3}$  and  $f_l \Rightarrow \tilde{f}_l$ .

For the Rees-Sciama effect, this is decomposed into only the  $l=0, l=1$ , and  $l=2$  Legendre coefficients:

$$\tilde{f}_0(k_1, k_2, \tau) = \frac{2(\tau_0 - \tau)\tau^2}{3} k_1 k_2 \left( \frac{17}{21} k_1 k_2 \right) \quad (25)$$

$$\tilde{f}_1(k_1, k_2, \tau) = \frac{2(\tau_0 - \tau)\tau^2}{3} k_1 k_2 \left( \frac{1}{2} (k_1^2 + k_2^2) \right) \quad (26)$$

$$\tilde{f}_2(k_1, k_2, \tau) = \frac{2(\tau_0 - \tau)\tau^2}{3} k_1 k_2 \left( \frac{4}{21} k_1 k_2 \right) \quad (27)$$

$$(28)$$

so,

$$l_3(l_3+1)B_{l_1 l_2 l_3} = \frac{1}{3\pi^4} \phi^2(\tau_r) \int d\tau \phi^2(\tau) (\tau_0 - \tau) \tau^2 \quad (29) \\ \times \int dk_1 dk_2 k_1^3 k_2^3 P(k_1) P(k_2) g(k_1) g(k_2) j_{l_1}(k_1 \tau_r) j_{l_2}(k_2 \tau_r) \\ \times \sum_{l' l''} j_{l'}(k_1 \tau) j_{l''}(k_2 \tau) (2l'+1)(2l''+1) \\ \times \left[ \frac{17}{21} Q_{0l'l'}^{l_1 l_2 l_3} k_1 k_2 + \frac{1}{2} Q_{1l'l'}^{l_1 l_2 l_3} (k_1^2 + k_2^2) + \frac{4}{21} Q_{2l'l'}^{l_1 l_2 l_3} k_1 k_2 \right]$$

As discussed in the appendix,  $\sum_{l' l''} (2l'+1)(2l''+1) Q_{l' l''}^{l_1 l_2 l_3} = (2l_1+1)(2l_2+1) Q_{0l_1 l_2}^{l_1 l_2 l_3}$ , and thus, if  $l$  is small (in this case, it only takes on the values 0,1,2), and  $h_{l' l''}$  is a function which varies slowly with  $l'$  and  $l''$ , we may make the approximation:

$$\sum_{l' l''} (2l'+1)(2l''+1) Q_{l' l''}^{l_1 l_2 l_3} h_{l' l''} \simeq (2l_1+1)(2l_2+1) Q_{0l_1 l_2}^{l_1 l_2 l_3} h_{l_2 l_1} \quad (30)$$



Under this assumption, the bispectrum reduces to:

$$\begin{aligned}
l_3(l_3 + 1)B_{l_1 l_2 l_3} &= \frac{4\phi^2(\tau_r)I_{l_1 l_2 l_3}}{3\pi^{5/2}} \int d\tau \phi^2(\tau)(\tau_0 - \tau)\tau^2 \\
&\times \int dk_1 dk_2 k_1^3 k_2^3 P(k_1)P(k_2)g(k_1)g(k_2) \\
&\times j_{l_1}(k_1\tau_r)j_{l_2}(k_2\tau_r)j_{l_2}(k_1\tau)j_{l_1}(k_2\tau)(k_1 + k_2)^2
\end{aligned} \tag{31}$$

where

$$I_{l_1 l_2 l_3} = \sqrt{(2l_1 + 1)(2l_2 + 1)(2l_3 + 1)} \begin{pmatrix} l_1 & l_2 & l_3 \\ 0 & 0 & 0 \end{pmatrix} \tag{32}$$

In order to deal with the spherical Bessel functions, we will first note that in the asymptotic limit, if  $x > l$ ,  $j_l(x) \simeq \sin(x - \pi l/2)/x$ . The lower limit of integration will be taken to be:

$$\tau_{min} = \max\left(\frac{l_1}{k_2}, \frac{l_2}{k_1}\right) \tag{33}$$

Likewise, the lower limit of integration on  $k_1$  is  $l_1/\tau_r$  and  $k_2$  is  $l_2/\tau_r$ . In this limit, we can expand out the four spherical Bessel functions as:

$$j_{l_1}(k_1\tau_r)j_{l_2}(k_2\tau_r)j_{l_2}(k_1\tau)j_{l_1}(k_2\tau) \simeq \frac{1}{4}(-1)^{l_1+l_2} \frac{\cos[(k_1 - k_2)\tau_r] \cos[(k_1 - k_2)\tau]}{k_1^2 k_2^2 \tau^2 \tau_r^2} \tag{34}$$

plus additional terms which oscillate much more quickly.

We can now approximate the the time integral:

$$\begin{aligned}
&\int_{\tau_{min}}^{\tau_r} d\tau \tau^2 (\tau_0 - \tau) \phi^2(\tau) j_{l_1}(k_1\tau_r) j_{l_2}(k_2\tau_r) j_{l_2}(k_1\tau) j_{l_1}(k_2\tau) \\
&\simeq \frac{1}{4}(-1)^{l_1+l_2} \cos[(k_1 - k_2)\tau_r] \int_{\tau_{min}}^{\tau_r} d\tau (\tau_0 - \tau) \phi^2(\tau) \frac{\cos[(k_1 - k_2)\tau]}{k_1^2 k_2^2 \tau^2} \\
&\simeq \frac{\pi}{4} \frac{\delta(k_1 - k_2)}{k_1^2 k_2^2 \tau_r^2} (-1)^{l_1+l_2} \phi^2(\tau_{min})(\tau_0 - \tau_{min})
\end{aligned} \tag{35}$$

where we have approximated  $\phi(\tau)(\tau_0 - \tau)$  as a slowly varying function which is maximally weighted near  $\tau = \tau_{min}$ , and  $\sin(x)/x$  is approximated as a delta function.

Thus, the bispectrum can be approximated as:

$$B_{l_1 l_2 l_3}^{(1)} \simeq \frac{\phi^2(\tau_r)}{\tau_r^2} \frac{4}{3\pi^{3/2}} \frac{I_{l_1 l_2 l_3}}{l_3(l_3 + 1)} \int_{l_m/\tau_r}^{\infty} dk k^4 P^2(k) g^2(k) \phi^2(\tau_{min}) (\tau_0 - \tau_{min}) \quad (36)$$

where we have defined  $l_m \equiv \max(l_1, l_2)$ .

In equation (8), we defined  $g(k)$  in terms of  $a_{lm}^L$ . Defining  $c_l \equiv \langle a_{lm}^L a_{lm}^{L*} \rangle$ , we find:

$$c_l = \frac{2}{\pi} \int k^2 dk P(k) j_l^2(k\tau_r) g^2(k) \quad (37)$$

For large values the spherical Bessel functions are very close to zero for  $k\tau_r < l$  and since  $k^2 P(k)$  is a monotonically decreasing function for all values of  $k$ , we may approximate  $j_l^2(x) = \pi\delta(l - x)/2$ . With this approximation:

$$c_{k\tau_r} \simeq \frac{\phi^2(\tau_r)}{\tau_r(2k/\tau_r + 1)} P(k) g^2(k) k^2 \quad (38)$$

Substituting this into the previous expression yields:

$$\begin{aligned} B_{l_1 l_2 l_3}^{(1)} &\simeq \frac{4}{3\pi^{3/2}\tau_r} \frac{I_{l_1 l_2 l_3}}{l_3(l_3 + 1)} \int_{k_{min}}^{\infty} dk k^2 P(k) c_{k\tau_r} (2k\tau_r + 1) \phi^2(\tau_{min}) (\tau_0 - \tau_{min}) \\ &\simeq \frac{4}{3\pi^{3/2}\tau_r^4} \frac{I_{l_1 l_2 l_3}}{l_3(l_3 + 1)} \sum_{l=l_m}^{\infty} l^2 (2l + 1) P\left(\frac{l}{\tau_r}\right) c_l \phi^2(\tau_r l_m/l) (\tau_0 - \tau_r l_m/l) \\ &\equiv \frac{4}{3\pi^{3/2}\tau_r^4} \frac{I_{l_1 l_2 l_3}}{l_3(l_3 + 1)} b_{l_m} \end{aligned} \quad (39)$$

In Figure 1 we have plotted the coefficient  $b_{l_m}$  for flat cosmologies where  $\Omega_m = 0.1, 0.3$ , and  $1.0$ .

Will we be able to detect this effect? We can estimate this by determining whether in a  $\Omega_m = 0.3, \Omega_\Lambda = 0.7$  universe, we can use the MAP data to reject the hypothesis that there is no non-Gaussianity in the CMB maps:

$$\chi^2 = \sum_{l_1, l_2, l_3} \frac{\langle B_{l_1, l_2, l_3} \rangle^2}{\langle B_{l_1, l_2, l_3}^2 \rangle} \quad (40)$$

In Figure 2 we show the amount of ‘‘information’’ gained by increasing the maximum index ( $l_3$  in our notation). Note that since all of the signal occurs around  $l < 600$ , and the MAP and PLANCK satellites are cosmic variance

dominated up to  $l \simeq 600$  and  $l \simeq 1000$  respectively, both experiments should measure the effect with approximately the same sensitivity.

The integral of Figure 2 gives us the total  $\chi^2$  between our fiducial model and some test model. In Figure 3, we plot the total  $\chi^2$  under the assumption that the “true” universe is a flat  $\Omega_m = 0.3$ , and the test models remain flat and vary  $\Omega_m$ . Even in the extreme case in which we assume  $\Omega_m = 0.3$  and the true universe has  $\Omega_m = 1.0$ , the  $\chi^2$  for PLANCK is only  $\sim 0.02$ .

## 5 Discussion

Most previous discussions of the microwave background have focused on multipole spectrum of the microwave background:

$$c_l = \frac{1}{2l+1} \sum_m a_{lm} a_{lm}^* \quad (41)$$

Because of azimuthal symmetry, the expectation value of  $\langle a_{lm}^2 \rangle$  is independent of  $m$ . If the microwave background fluctuations were purely a Gaussian random field, then the multipole spectrum measures all of the statistical properties of the microwave background.

In this paper, we have developed formalism for computing the bispectrum and for measuring it from microwave background maps. As an example, we computed the Rees-Sciama bispectrum and found that is undetectable with current and forthcoming missions. In a companion paper[14], we will work out the bispectrum for nonlinear contributions from the coupling of gravitational lensing and low-redshift temperature perturbations. There, we show that MAP will be able to detect the SZ-lensing bispectrum and PLANCK will be able to detect the ISW-lensing bispectrum.

Much work remains to be done on the bispectrum. We do not have a robust statistical technique for computing the bispectrum from a million pixel map with sky cuts and spatially variable noise, nor do we understand how foregrounds will contaminate measurements of the bispectrum. For example, with MAP, radio sources are expected to produce marginally detectable skewness[15]. There are also other physical effects that may have observable signatures in the bispectrum.

## 6 Acknowledgments

We thank Martin Bucher, Jeremy Goodman, Gary Hinshaw, Arthur Kosowsky and Jim Peebles for useful discussions. DNS acknowledges the MAP/MIDEX project for support. DMG is supported by an NSF graduate research fellowship.

## 7 References

### References

- [1] A. Kogut, A.J. Banday, C.L. Bennett, K.M. Gorski, A. Kogut, G.F. Smoot & E.L. Wright, *Astrophys. J. Lett.*, **464**, L11 (1996).
- [2] P.G. Ferreira, J. Magueijo, & K.M. Gorski, *Astrophys. J. Lett.*, **503**, L1 (1998).
- [3] A.F. Heavens, *MNRAS*, **299**, 805 (1998).
- [4] C.L. Bennett, M. Halpern, G. Hinshaw, N. Jarosik, M. Limon, J. Mather, S.S. Meyer, L. Page, D.N. Spergel, G. Tucker, D.T. Wilkinson, E. Wollack, E.L. Wright, *Bull. Amer. Astron. Soc.*, 191.8701, (1998), <http://map.gsfc.nasa.gov>.
- [5] <http://astro.estec.esa.nl/PLANCK/>
- [6] T. Falk, R. Rangarajan and M. Srednick, *Astrophys. J. Lett.*, **403**, L1 (1993).
- [7] P.J.E. Peebles, *The Large Scale Structure of the Universe*, Princeton University Press (1980).
- [8] T. Pyne and S.M. Carroll, *Phys. Rev. D* **53**, 2920 (1996).
- [9] S. Mollerach and S. Matarrese, *Phys. Rev. D* **56**, 4494 (1997).
- [10] S. Mollerach, A. Gangui, F. Lucchin and S. Matarrese, *Astrophys. J.*, 453, 1 (1995).

- [11] D. Munshi, T. Souradeep, and A. A. Starobinsky, *Astrophys. J.*, 454, 552 (1995).
- [12] X. Luo, *Astrophys. J. Lett.*, 427, L71 (1994).
- [13] U. Seljak, *Astrophys. J.*, **460**, 549 (1996).
- [14] D. M. Goldberg & D. N. Spergel, Submitted to *Phys. Rev. D* (1998).
- [15] A. Refregier, D. N. Spergel, & T. Herbig, to appear in *Astrophys. J.* (1998).
- [16] D.A. Varshalovich, A.N. Moskalev, Y.K. Khersonskii, *Quantum Theory of Angular Momentum: Irreducible Tensors, Spherical Harmonics, Vector Coupling Coefficients, 3nj Symbols*, World Scientific: Singapore, p454 (1988).

## A Wigner Symbol Identities

In this appendix, we derive some relevant properties for the integral,

$$\begin{aligned}
Q_{ll'l''}^{l_1 l_2 l_3} &\equiv \int d\hat{l} d\hat{m} d\hat{n} P_l(\cos \alpha) P_{l'}(\cos \beta) P_{l''}(\cos \gamma) \\
&\quad \times \sum_{m_1, m_2, m_3} \begin{pmatrix} l_1 & l_2 & l_3 \\ m_1 & m_2 & m_3 \end{pmatrix} Y_{l_1 m_1}^*(\hat{l}) Y_{l_2 m_2}^*(\hat{m}) Y_{l_3 m_3}^*(\hat{n}) \\
&= \left( \frac{4\pi}{2l+1} \right) \left( \frac{4\pi}{2l'+1} \right) \left( \frac{4\pi}{2l''+1} \right) \sum_{m_1, m_2, m_3} \begin{pmatrix} l_1 & l_2 & l_3 \\ m_1 & m_2 & m_3 \end{pmatrix} \\
&\quad \times \sum_{m, m', m''} \int d\hat{l} d\hat{m} d\hat{n} Y_{lm}(\hat{l}) Y_{l'm'}^*(\hat{m}) Y_{l''m''}(\hat{n}) Y_{l'm''}^*(\hat{n}) Y_{l''m''}(\hat{n}) Y_{l'm''}^*(\hat{l}) \\
&\quad \quad \quad \times Y_{l_1 m_1}^*(\hat{l}) Y_{l_2 m_2}^*(\hat{m}) Y_{l_3 m_3}^*(\hat{n}) \\
&= I_{ll'l''}^{l_1 l_2 l_3} \sum_{m_1, m_2, m_3} \begin{pmatrix} l_1 & l_2 & l_3 \\ m_1 & m_2 & m_3 \end{pmatrix} \sum_{m, m', m''} \begin{pmatrix} l & l'' & l_1 \\ m & -m'' & -m_1 \end{pmatrix} \\
&\quad \begin{pmatrix} l' & l & l_2 \\ m' & -m & -m_2 \end{pmatrix} \begin{pmatrix} l'' & l' & l_3 \\ m'' & -m' & -m_3 \end{pmatrix} (-1)^{(m+m'+m'')} \quad (42)
\end{aligned}$$

where  $\cos \alpha = \hat{l} \cdot \hat{m}$ ,  $\cos \beta = \hat{m} \cdot \hat{n}$  and  $\cos \gamma = \hat{l} \cdot \hat{n}$  and

$$I_{l'l''}^{l_1 l_2 l_3} = \sqrt{(4\pi)^3 (2l_1 + 1)(2l_2 + 1)(2l_3 + 1)} \begin{pmatrix} l & l'' & l_1 \\ 0 & 0 & 0 \end{pmatrix} \begin{pmatrix} l' & l & l_2 \\ 0 & 0 & 0 \end{pmatrix} \begin{pmatrix} l'' & l' & l_3 \\ 0 & 0 & 0 \end{pmatrix} \quad (43)$$

We can use the definition of the Wigner 6-j symbol[16] to rewrite the integral as,

$$\begin{aligned} Q_{l'l''}^{l_1 l_2 l_3} &= I_{l'l''}^{l_1 l_2 l_3} \begin{Bmatrix} l_1 & l_2 & l_3 \\ l' & l'' & l \end{Bmatrix} (-1)^{l+l'+l''} \sum_{m_1, m_2, m_3} \begin{pmatrix} l_1 & l_2 & l_3 \\ m_1 & m_2 & m_3 \end{pmatrix}^2 (-1)^{l_1+l_2+l_3} \\ &= I_{l'l''}^{l_1 l_2 l_3} \begin{Bmatrix} l_1 & l_2 & l_3 \\ l' & l'' & l \end{Bmatrix} (-1)^{l+l'+l''} \end{aligned} \quad (44)$$

If  $l'' = 0$ , then the only non-zero term is

$$Q_{l_1 l_3 0}^{l_1 l_2 l_3} = \sqrt{\frac{(2l_2 + 1)(4\pi)^3}{(2l_1 + 1)(2l_3 + 1)}} \begin{pmatrix} l_1 & l_2 & l_3 \\ 0 & 0 & 0 \end{pmatrix} \quad (45)$$

If  $l'' = 1$ ,  $Q_{l'l_1}^{l_1 l_2 l_3}$  is zero unless  $l = l_1 \pm 1$  and  $l' = l_3 \pm 1$ . Thus, there are only four terms in the sum in equation (27).

We can evaluate these terms by noting that

$$\begin{pmatrix} l_1 - 1 & l_2 & l_3 - 1 \\ 0 & 0 & 0 \end{pmatrix} = \sqrt{\frac{(l_1 + l_2 + l_3 + 1)(l_1 - l_2 + l_3)}{(l_1 + l_2 + l_3)(l_1 - l_2 + l_3 - 1)}} \begin{pmatrix} l_1 & l_2 & l_3 \\ 0 & 0 & 0 \end{pmatrix} \quad (46)$$

$$\begin{pmatrix} l_1 & l_1 - 1 & 1 \\ 0 & 0 & 0 \end{pmatrix} = -\sqrt{\frac{l_1}{(2l_1 + 1)(2l_1 - 1)}} \quad (47)$$

and

$$\begin{Bmatrix} l_1 & l_2 & l_3 \\ l_3 - 1 & 1 & l_1 - 1 \end{Bmatrix} = \sqrt{\frac{(l_1 + l_2 + l_3 + 1)(l_1 + l_2 + l_3)(l_1 - l_2 + l_3 - 1)(l_1 - l_2 + l_3)}{(2l_1 + 1)2l_1(2l_1 - 1)(2l_3 + 1)2l_3(2l_3 - 1)}} \quad (48)$$

Thus we can reduce the product of Wigner symbols to a simpler form:

$$Q_{l_1-1, l_3-1, 1}^{l_1 l_2 l_3} = \frac{(l_1 + l_2 + l_3 + 1)(l_1 - l_2 + l_3)}{2(2l_1 - 1)(2l_3 - 1)} Q_{l_1 l_3 0}^{l_1 l_2 l_3} \quad (49)$$

Similarly,

$$Q_{l_1+1, l_3-1, 1}^{l_1 l_2 l_3} = \frac{(l_1 + l_2 - l_3 + 1)(-l_1 + l_2 + l_3)}{2(2l_1 + 3)(2l_3 - 1)} Q_{l_1 l_3 0}^{l_1 l_2 l_3}, \quad (50)$$

$$Q_{l_1-1, l_3+1, 1}^{l_1 l_2 l_3} = \frac{(-l_1 + l_2 + l_3 + 1)(l_1 + l_2 - l_3)}{2(2l_1 - 1)(2l_3 + 3)} Q_{l_1 l_3 0}^{l_1 l_2 l_3}, \quad (51)$$

and

$$Q_{l_1+1, l_3+1, 1}^{l_1 l_2 l_3} = \frac{(l_1 + l_2 + l_3 + 2)(l_1 - l_2 + l_3 + 1)}{2(2l_1 + 3)(2l_3 + 3)} Q_{l_1 l_3 0}^{l_1 l_2 l_3}, \quad (52)$$

Note that

$$\sum_{l'} Q_{l' l_1}^{l_1 l_2 l_3} (2l + 1)(2l' + 1) = (2l_1 + 1)(2l_3 + 1) Q_{l_1 l_3 0}^{l_1 l_2 l_3}, \quad (53)$$

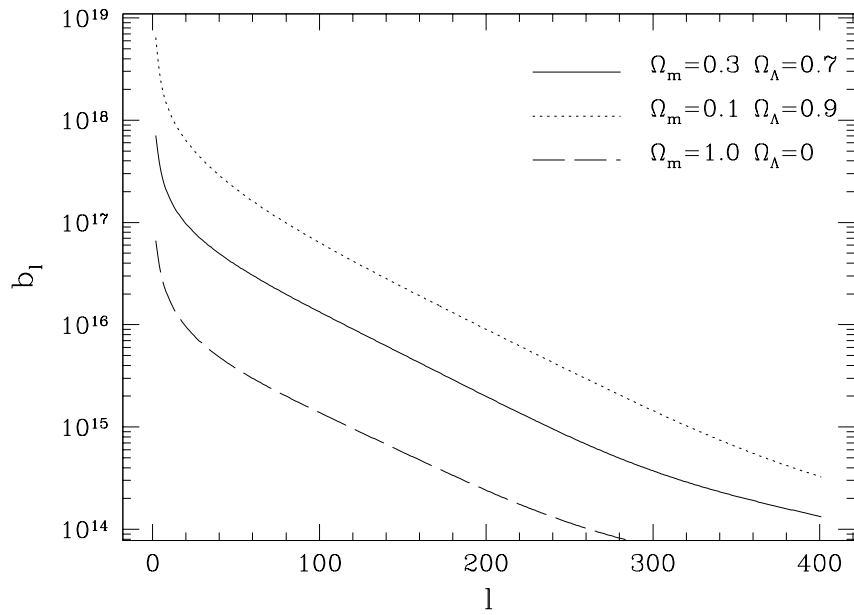


Figure 1: The coefficients  $b_{l_m}$  for various cosmologies, as defined in the text. Note that for low  $\Omega$  models, the signal is significantly larger than  $\Omega_m = 1$  models at all  $l$ .



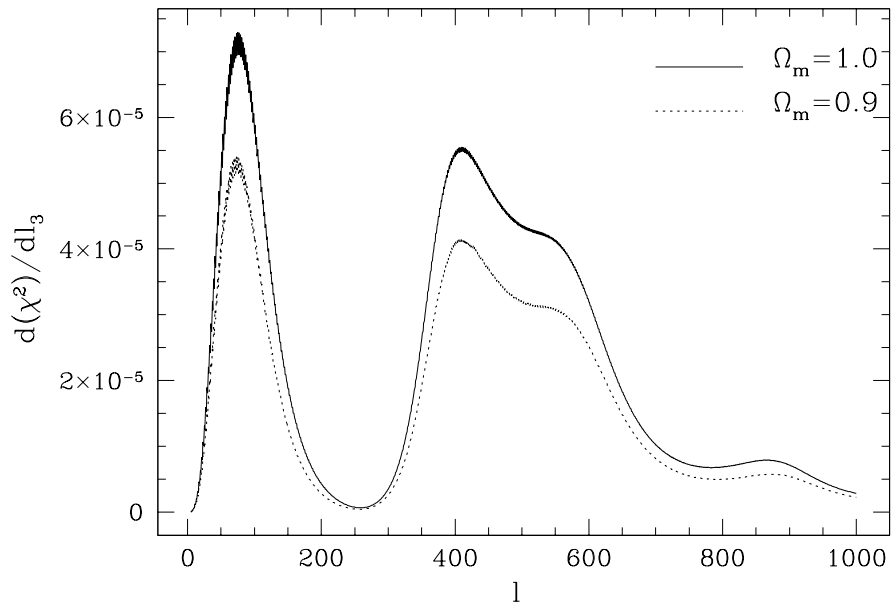


Figure 2: The amount of information gained by increasing  $l_3$ , as given by  $\chi^2 = \sum (\langle B_{l_1 l_2 l_3}(\Omega_m) \rangle - \langle B_{l_1 l_2 l_3}(\Omega_m = 0.3) \rangle)^2 / \langle B_{l_1 l_2 l_3}^2 \rangle$ , where we have used the PLANCK detection sensitivity. Since there is very little contribution above  $l_3 = 700$ , the MAP and PLANCK missions will be equally sensitive to this effect. Our fiducial model here and throughout is  $\Omega_m = 0.3$ ,  $\Omega_\Lambda = 0.7$ . The shape of this spectrum comes from several competing effects. At large  $l$ , more modes are included in the sum, providing a larger signal. However, the signal per mode becomes increasingly weak at a logarithmic rate for high  $l$ , as suggested by the plot of the coefficients in Figure 1. Finally, the features in the spectrum above are caused by variations in the expected noise. Troughs correspond to peaks in the CMB spectrum.

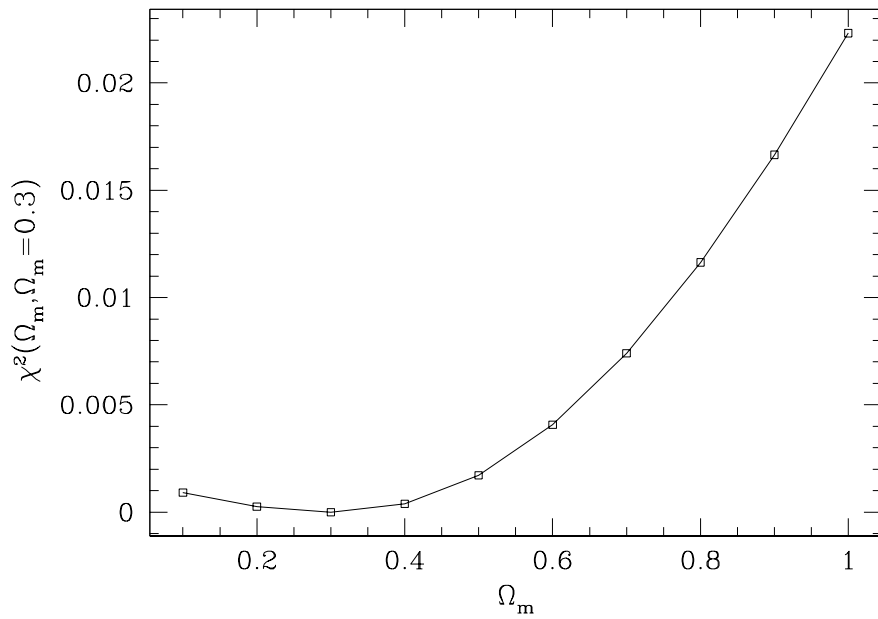


Figure 3: The total value of  $\chi^2(\Omega_m, \Omega_m = 0.3)$  for variations in  $\Omega_m$  for both PLANCK and MAP. All values of  $\Omega_m$  produce signals which are consistent with  $\Omega_m = 0.3$ .